



ON-LINE SAMPLING AND INTACT MASS ANALYSIS OF NANOMETER-SIZE AEROSOLS VIA TIME-OF-FLIGHT HIGH-MASS SPECTROMETRY

Marcos M. Alvarez, Igor Vezmar and Robert L. Whetten*

School of Physics and Chemistry, and Microelectronics Research Center, Georgia Institute of Technology,
Atlanta, GA 30332-0430, U.S.A.

(First received 26 June 1996; and in final form 17 June 1997)

Abstract—A device capable of continuously sampling and mass analyzing aerosols in the 1-10 nm diameter size range (masses up to 1 MDa) at part per billion (ppb, 10^{10} cm^{-3}) concentrations is described. Small aliquots of an aerosol flowing at atmospheric pressure are sampled into a time-of-flight mass spectrometer (TOFMS) via a pulsed molecular beam valve at 10–50 Hz. The aerosol molecular beam is singly and nondestructively ionized with light from an ultraviolet excimer laser and accelerated across a 20 kV electrostatic field. Ionized particle packets are separated in mass during a free flight and re-accelerated across an additional 30 kV into a stainless steel conversion dynode plate. Signals from ejected electrons and negative ion fragments resulting from the particle-dynode collisions are amplified in a dual microchannel plate detector, digitized, and stored in a fast transient recorder. Sampling of He flow streams bearing benzene, fullerenes, as well as Na, Mg, and CsI particles (nanocrystals) is demonstrated. In addition, the gas-phase reaction between a pre-formed Na nanocrystal and alkane thiols is monitored in real-time. © 1998 Elsevier Science Ltd. All rights reserved

INTRODUCTION

The real-time monitoring of submicron aerosols is a powerful tool with potential applications in the study of aerosol formations, reactions, and dynamics, as well as in monitoring of environmental pollutants and industrially important aerosols (Kaye and Trotter, 1995). Techniques for the real-time sizing and chemical characterization of individual micron-size particles with sensitivities of 10^2 cm^{-3} are now available. They use light scattering to detect presence and size of a single particle. Subsequent decomposition of examined particles into their elemental or molecular constituents is done by heating (Sinha and Friedlander, 1985) or use of synchronized laser pulse (Marijnissen *et al.*, 1988; McKeown *et al.* 1991; Nordmeyer and Prather, 1994; Thomson, 1994; Carson *et al.*, 1995; Hinz *et al.*, 1995; Weiss *et al.*, 1995; Reilly *et al.*, 1997). Ionized pyrolysis products are detected using mass spectrometry. However, submicron particles are not easily detected with these techniques due to their small light scattering efficiencies.

Nanometer-size particles (1-10 nm diameters) are too small for classical sizing techniques based on light scattering and too large for conventional mass spectrometers used in on-line monitoring of molecular species, such as GC/MS, LC/MS, and HPLC/MS (Arpino, 1995). As a result, light scattering is used to characterize nanometer size aerosols only in conjunction with condensation particle counters (Wiedensohler *et al.*, 1994), while the use of mass spectrometry is typically restricted to the analysis of elemental or molecular particle ablation products (Reents *et al.*, 1995). Therefore, diffusion batteries (Wiedensohler *et al.*, 1994), ion-mobility analyzers, and electrostatic analyzers (Wang and Flagan, 1990; Winklmayr *et al.*, 1991; Makela and Jokinen, 1994) remain the methods of choice for the characterization of ultra-fine particles. Recently, the particle beam mass spectrometer (Ziemann *et al.*, 1995), the atmospheric pressure chemical ionization mass spectrometer, and the Kelvin effect sizing schemes (Weber *et al.*, 1995) have been developed. These instruments, while highly successful in sizing particles in the 1-1000 nm size regime at very low

*Author to whom correspondence should be addressed

concentrations ($< 100 \text{ cm}^{-3}$), require scanning of an electrostatic field during analysis. This is limiting their use in monitoring instantaneous changes in aerosol processes.

In principle, mass spectrometry enables the mass analysis of intact submicron particles. Particularly, TOFMS offers the advantage of operational simplicity, mass-independent resolution, unlimited mass range, and a microsecond time scale of analysis amenable to real-time monitoring of aerosol processes (Cotter, 1992; Guilhaus, 1995; Weber *et al.*, 1995). A mass spectrum of an aerosol provides information on size through knowledge of densities and expected structures, on composition through the elucidation of fragmentation patterns, and on relative abundance of aerosol components. The benefits of such information in small particle research can be gauged, for instance, by its essential role in unveiling the electronic shell structure in metal clusters (de Heer, 1993), and in elucidating the uniqueness of fullerenes among other species in carbon cluster beams (Kroto *et al.*, 1985).

In practice, two factors limit the applicability of mass spectrometry to the continuous real-time sampling of submicron aerosols at atmospheric pressures. First, the coupling of a high pressure aerosol to a low-vacuum mass spectrometer chamber requires a multi-stage pumping system. Secondly, and more significantly, even the smallest particles have masses of thousands of Daltons, mass range in general difficult to detect in conventional spectrometers. Since the early seventies, clusters generated in gas aggregation sources have been coupled to TOFMS operating at high voltages (Sattler *et al.*, 1980). It is now possible to detect intact large particles with masses into the MDa range (Murray *et al.*, 1994; Zimmermann *et al.*, 1994).

Motivated by the need to monitor the growth and evolution of nanocrystals in an aerosol flow processor, we have developed a device capable of sampling and mass analyzing nanometer-size aerosols on a millisecond time scale. The instrument circumvents the high-pressure-to-vacuum interface problem by pulse sampling only a minute portion of an aerosol into a high-vacuum mass spectrometer. High-mass detection is enhanced by operating the acceleration and detection regions of the mass spectrometer at high voltages (40-50 kV). We report on the capability of the instrument to sample a variety of materials and to characterize different conditions affecting particle size in an aerosol source. In addition, the real-time monitoring of the gas-phase reaction between a pre-formed Na nanocrystals and alkane thiols is demonstrated.

EXPERIMENTAL DETAILS

The apparatus is comprised of a multi-stage nanocrystal flow processor (NXFP), a sampling interface, and a TOFMS (Figs 1 and 2).

Aerosol source

Aerosols of fullerenes and metal particles are generated in a Nanocrystal Flow Processor described in detail elsewhere (Alvarez, 1995). Nanoparticles are produced in a source stage (A) by evaporating the material of interest into a flowing carrier gas stream (typically He) and slowly cooling it in an aggregation cell. The emerging nanocrystal aerosol is then immediately diluted with a secondary He stream; the dilution stream is either neat or seeded with an appropriate passivating or etching chemical agent. The chemical agent is generated in a temperature-controlled passivation cell (B) by evaporating it into the secondary He stream. Both streams, flowing slightly above atmospheric pressure, meet at the dilution or mixing stage (C). A minute portion of the rarefied or passivated aerosol is then non-destructively sampled via a special molecular pulse beam valve (D) into a high-mass TOFMS for further characterization. The majority of the aerosol flows to a collection stage (E) or to other processing stages such as etching, annealing, and passivation. Benzene bearing streams are generated by bubbling He through liquid benzene in a conventional gas bubbler.

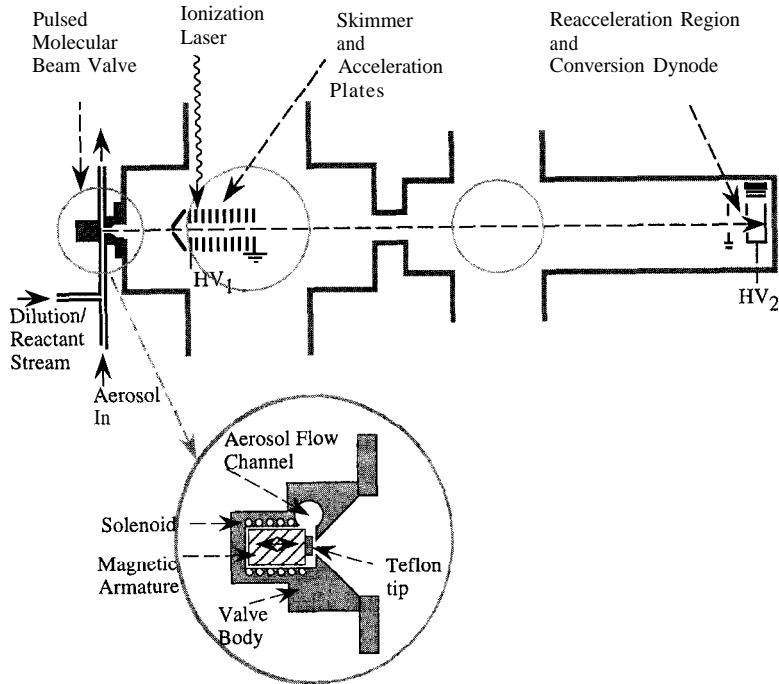


Fig. 1. Schematic diagram of the TOFMS and aerosol sampling valve. A flowing atmospheric aerosol is extracted into a high vacuum chamber via a pulsed molecular beam valve. In vacuum, the most intense part of the beam is collimated through a skimmer. The aerosol then flows into the acceleration region of the mass spectrometer where it is ionized by a synchronized laser beam and accelerated across a high electrostatic potential (HV₁). After traveling through a free flight region, separated ion packets are post accelerated into a stainless steel dynode plate held at a negative high voltage HV₂. Fragmented anions or generated electrons are subsequently accelerated into a dual microchannel plate detector.

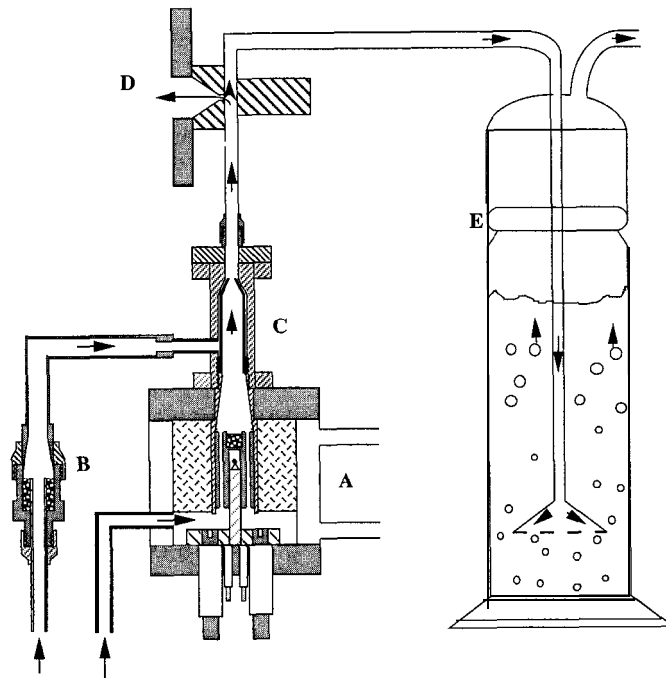


Fig. 2. Schematic diagram of a NXFP. The device consists of a nanocrystal source (A), passivation agent source (B), aggregation cell and dilution or mixing region (C), a sampling interface (D), and collection device (E).

Aerosol sampling

A modified commercial molecular beam valve (General Valve) is used as a sampling interface between the NXFP and the mass spectrometer. The unit generates pulses at least 200 μs wide at repetition rates up to 1 kHz using a General Valve Iota I pulse driver. The modification consists of sealing the conventional inlet port of this unit and welding a 10 mm OD flow pipe tangent to the valve's internal chamber that houses solenoid, tip, and orifice as shown in Fig. 1. Effectively, the flow pipe is part of the molecular beam valve. The Teflon sealing tip restricts the operational temperature to a maximum of 200°C, above which the material softens. A 1 mm OD orifice in the flow pipe discharges directly at the valve's nozzle, delivering the aerosol to the valve.

Only a minute portion of the aerosol is pulsed into the mass spectrometer. Although the throughput in the flow processor is high, 10 bar-l/min, this flow is active only for 500 μs . As a result, the gas loading to the mass spectrometer chambers (0.05 bar-l/min, at 10 Hz) is small enough to be controlled with a small two-stage pumping system, 300 l/s, each. The aerosol expands near sonic velocities of 1.5×10^5 cm/s for He into the mass spectrometer vacuum, discharging approximately 1 cm³ of aerosol per pulse (cross sectional area of 0.01 cm² for a period of 500 μs). Since the stagnation volume of the valve is only 100 μl , fresh sample is released in each cycle. In the studies described here, particle concentrations of ppb are typical; thus on the order of 10^{10} particles are allowed into the mass spectrometer per pulse. The transient aerosol pulse, as monitored via a fast ion gage at a fixed distance from the valve's nozzle is approximately of Gaussian shape with a FWHM of 500 μs . In vacuum, the aerosol stream emerges as a molecular beam. Its central part is collimated by a 3 mm skimmer, 5 cm away from the valve's nozzle and flows through the center axis of the mass spectrometer.

Mass spectrometer

The TOFMS (Fig. 1) consists of an acceleration/ionization region, a field free region, and a detection stage.

When the aerosol pulse reaches the acceleration plate assembly of the mass spectrometer, it is ionized by a laser beam. The region of ionization is typically 1 mm wide and 1 cm high. The fluence of the ionization laser is adjusted by inserting quartz attenuation plates in its path in order to exclude multiple ionization and photofragmentation. This is judged by the absence of low mass species in the mass spectra and by the absence of mass spectral peaks at rational fractions (doubly charged, triply charged, etc.) of the singly charged parent mass. The time period between the valve opening and the firing of the ionization laser is monitored and controlled by a commercial time delay generator (Stanford Research Systems, DG535). Typically, the ionization laser is synchronized with the pulsed valve so that the laser is fired when the central part of the aerosol pulse is present in the ionization region of the mass spectrometer so as to minimize transient effects occurring at the edges of the aerosol pulse.

As the laser pulse ionizes the particles, the resultant positively charged particles are instantaneously accelerated across a large electrostatic potential difference, HV_1 of up to 20 kV, toward a charge particle detector. Ions emerge out of the acceleration region with approximately the same kinetic energy but with velocities inversely proportional to their masses. Once in the field-free region, this difference in particle velocity translates into a difference in time of arrival at a detector located 1.2 m away. A set of dual microchannel plates is commonly used for particle detection. However, such detector is inefficient in detecting massive particles. Therefore massive particles are detected indirectly by allowing them to collide with a surface of a conversion dynode and subsequently detecting the negative ion fragments and electrons. To impart sufficient kinetic energy to the particles before collision with the dynode, discrete ion packets are reaccelerated across a large negative potential, HV_2 , typically 30 kV. The conversion dynode is essentially a pre-amplifier onto which positive ions are accelerated from ground down to HV_2 . Electrons and

negative ion fragments resulting from the particle-dynode collision are accelerated perpendicularly toward a dual microchannel plate detector. Resulting amplified currents are first converted to voltage pulses in a fast 100 MHz preamplifier before they are digitized and averaged in a transient recorder (LeCroy).

The acceleration and detection assemblies are housed in two different vacuum chambers isolated by a 2.5 cm OD gate valve. Each chamber is evacuated with a 300 l/s turbomolecular pump (Varian, V-300). Operating pressures are 1×10^{-5} mbar and 2×10^{-6} mbar, respectively, during aerosol sampling. In the high-mass detection mode when high acceleration voltages are used, the resolution of the instrument is 40. To detect lighter masses it is sufficient to operate the instruments at lower acceleration voltages (5 kV) and to use conventional dual microchannel plate assembly as detector. Resolution in that case is 500.

Benzene and fullerene mass spectra are obtained using a regular dual microchannel plate detector. Large particles are detected using high voltage acceleration and conversion dynode as a pre-amplification stage. All aerosols reported here are ionized with 193 nm light from an ArF excimer laser.

CHARACTERIZATION

The ability of the instrument to sample various materials is illustrated in Fig. 3. The mass spectra of He streams containing benzene, fullerenes, and CsI nanocrystals are shown. Benzene and fullerenes serve as convenient time and mass calibration standards because they are stable molecules easily ionized with two 193 nm photons from an ArF excimer laser. In addition to the materials shown in Fig. 3, aerosols of Na, Mg, and NaCl were routinely analyzed. In theory, there is no fundamental restriction on what materials are amenable to sampling and detection with the present scheme. In practice, however, particles of materials with ionization potentials higher than the energy of the ionizing laser can not be detected in this instrument without significant particle fragmentation. In addition, the

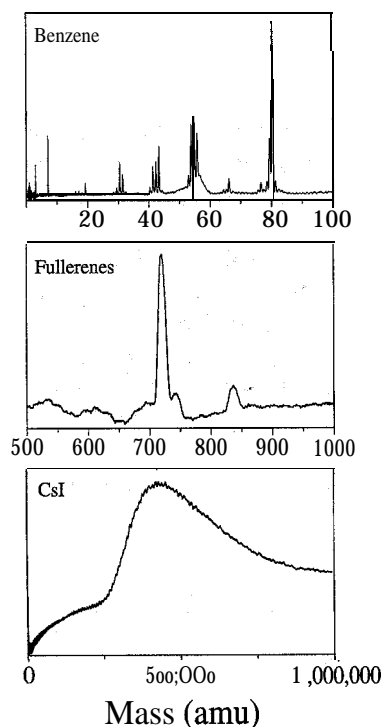


Fig. 3. Aerosol sampling: (a) benzene and its photofragments, (b) fullerene extract, (c) a large CsI nanocrystal of approximately 1700 salt units, 5.5 nm in diameter.

difficulty in detecting larger masses even if employing a high-voltage acceleration and conversion dynode detection, limits the mass of detectable particles to 1 MDa.

Instrumental sensitivity

In general, nanocrystal aerosols are detected in the experimental configuration shown in Fig. 1, when the monomer vapor pressure in the aerosol source (Fig. 2, A) is around 0.1 mbar. Since the mass spectra reports a mean aerosol mass, an estimate of the particles' maximum concentration in the carrier gas is obtained by dividing the monomer vapor mole fraction by the number of units in the particle. The minimum vapor pressure and hence the furnace temperature at which signal is registered in the mass spectrometer is thus a measure of the minimum instrumental sensitivity. Systematic measurements of the appearance threshold for Na, Mg, and CsI particles are shown in Table 1. Values reported in the table should be taken as lower bounds since material losses to the walls of the flow system prior to sampling are neglected. It is also assumed that a single particle mass is produced.

Minimum detection thresholds are found to be on the order of ppb (10^{10} cm^{-3}). Although, by far higher than those reported with ion mobility analyzers ($< 100 \text{ cm}^{-3}$), the sensitivity of the instrument suffices to characterize our aerosol source and most particle sources reported in the literature (Haberland, 1994). It is instructive, at least qualitatively, to enumerate the factors responsible for such low sensitivity; namely: (i) the volume fraction of the aerosol pulse actually probed by the ionization laser, (ii) ionization efficiency, (iii) ion transmission efficiency from the ionization region to the mass spectrometer detector; and (iv) detector efficiency.

Let us assume that approximately 10^{10} particles are discharged into the mass spectrometer per aerosol pulse. An upper bound estimate of the aerosol pulse fraction actually interrogated by the ionization laser may be obtained by assuming that the aerosol expands into the vacuum chamber at sonic velocities, which is $1.5 \times 10^5 \text{ cm/s}$ for He, defining a cone whose dimensions are determined by the valve's conical expansion 20" nozzle. For a typical pulse duration of 500 μs , this volume is approximately $50,000 \text{ cm}^3$, a 75 cm long cone with a base diameter of 50 cm. Since a 20 ns laser pulse probes only 1 cm^3 of this volume, the volume fraction of gas actually sampled is only 2×10^{-5} . Therefore, the number of particles subject to ionization in one pulse is in the order of 10^5 . Although resulting in a considerable loss in sensitivity, aerosol dilution is necessary to ensure that the sampled particles will not grow by particle-particle collisions as they travel from the source to the ionization region.

Experimental measurements of absolute cluster ionization cross sections or efficiencies are virtually non-existent. With a lack of absolute data, it is typically assumed that photoionization cross sections follow an additive rule, increasing linearly with the number of atomic constituents (Mark and Echt, 1994). Invoking this approximation, we estimate that a 1 nm particle has a maximum ionization cross section on the order of 10^{-14} cm^2 . With particle densities of 10^5 cm^{-3} in the ionization region, approximately 10^3 particles will be ionized with 6.4 eV light from -5 μJ laser pulse. Therefore, a maximum ionization efficiency is around 10^{-2} , which agrees with photoelectric yields of a few percent observed for large metallic particles (Burtscher and Siegmann, 1994). It should be noted that the ionization process in our system is different from the photoelectric charging of aerosols at ambient pressures since the probability of photoelectrons diffusing back onto the particle

Table 1. Minimum sampling sensitivity for various materials

Material	Monomer vapor pressure (mbar)	Number of monomer units	Particle diameter (nm)	Concentration (10^{10} cm^{-3})
Cesium iodide	0.002	2000	6	1
Magnesium	0.1	2500	5	50
Sodium	0.09	8000	8	15

surface and neutralizing it is very low. The low ionization probability and low particle density in the ionization region of the mass spectrometer ensures that particles are singly ionized, as observed by absence of multiple peaks in mass spectra. Low ionization efficiency does not place a significant limitation on the analysis of most metallic particles, but will hinder the analysis of organic aerosols whose ionization potentials may exceed 10 eV. If a mixture of particles with different ionization potentials is analyzed, the mass spectra will be biased toward the materials with lower ionization potentials. When necessary, these limitations may be avoided by using a vacuum ultraviolet ionization source (Bahat *et al.*, 1987) or electron impact ionization which is less sensitive to particle composition. However, since the nanocrystals studied here have ionization potentials below the energy of ionization laser, it is expected that the ionization process is not severely deteriorating the relative sensitivity.

To achieve high mass resolution, most mass spectrometers are designed to extract ions in a direction perpendicular to their original motion. Since it is difficult to electrostatically deflect massive particles, such instruments suffer from low ion transmission efficiencies and mass discrimination (Zimmermann *et al.*, 1994). However, since the pulse valve, acceleration plates, and detector of our mass spectrometer are along the same axis (Fig. 1), it is expected that the ion extraction efficiency is nearly unity, independent of particle size and composition. The trade-off is a loss in the resolution.

High-mass detection demands higher ion acceleration and post-acceleration (conversion dynode) voltages than those required in conventional mass spectrometers, which typically employ channeltron or microchannel plate assemblies for ion detection. The latter are highly efficient in detecting photons (5510%) and light ions (> 60%) (Siegmond and Malina, 1983). However, their efficiency in detecting massive particles drastically decreases with particle size. For instance, the activation energy for detecting very large metal clusters of Cs, Na, and Li was found by Zimmermann and collaborators to be 8 eV/atom. Hence, a 2000-atom Na particle must be accelerated to at least 16 kV for its non-biased detection. Due to technical difficulties in floating microchannel plates at voltages in excess of 10 kV, a conversion dynode plate is used for large ion detection (Daley, 1960; Bahat *et al.*, 1987). These devices have a limited mass range, limited by a particle velocity detection threshold which is on the order of 10^4 m s^{-1} (Haberland, 1994). In such cases, a 2000-atom Na particle must be accelerated to an unrealistic potential of 500 kV to be detected. Our experience in detecting gold nanocrystals by laser desorption mass spectrometry (Alvarez, 1995; Vezmar *et al.*, 1997) with a stainless steel conversion dynode reveals a relative detection threshold of 40 eV/atom, a number much higher than the values reported for alkali metals. These measurements depend on the particular instrument configuration used, the type of material being analyzed, as well as the dynode surface under consideration. Indeed, CsI crystals have a higher sensitivity (Table 1) because they are easier to detect. As most ionic solids, CsI crystals are easily broken into ion fragments upon collision with the conversion dynode surface (with as little as 1 eV/atom energy) (Whetten, 1993). We have not performed a quantitative study of the detector's efficiency, but have estimated an upper bound particle detection efficiency on the order of 10^{-2} , based on typical microchannel plate efficiencies for detecting light ions (Siegmond and Malina, 1983). Out of the 10^3 particles striking the detector, approximately 10 particles are actually detected. The small number is not a surprising, since it should be possible to detect a single particle striking the dynode surface since a large number of ions and electrons are ejected following particle fragmentation.

Resolution

The high-voltage detection approach used here suffers from the disadvantage of demanding a large energy threshold for particle detection and of exhibiting a sensible loss of resolution. The instrumental resolution is seriously affected by the difficulty of applying uniform fields at high electrostatic potential in a limited space where just preventing arcing is a considerable feat. Furthermore, the particle fragmentation times upon

colliding with the dynode may be of the order of milliseconds, hence affecting the time-of-flight measurement. An additional time spread arises from the particle fragments time-of-flight in traveling the 4 cm distance between their point of origin and the microchannel plate detector. All these factors contribute to the reduction of resolution from 500 to 40 when switching to high voltage detection.

In the following discussion, two assumptions are made; particles acquire the same initial velocity when expanding into vacuum, and the sampling process is insensitive to particle size. These assumptions made are approximations since it is expected that by the virtue of their different aerodynamic diameters and inertia, particles will acquire different final velocities upon expanding into vacuum (Zimmermann *et al.*, 1994). In fact, for micron-size particles this effect is used in conjunction with light scattering to determine particle size (Nordmeyer and Prather, 1994). The variation in initial velocity will not affect the resolution of the instrument but will interfere with its mass calibration, which assumes that the particle time-of-flight velocity is determined solely by the energy added electrostatically. This velocity slip might result in size selectivity. Zimmermann and collaborators have quantified such an effect in their gas aggregation source. For a 100 kDa Na nanocrystal, they find a typical velocity variation of 30% relative to that of the carrier gas. We have not characterized such effect in our instrument. An effect of the same order of magnitude is assumed to show that the velocity slip has a negligible impact on both the sampling selectivity and the instrument mass calibration.

In the system described here, it takes approximately 200 μs for an instantaneous aerosol pulse to transverse the region between the valve's nozzle and the ionization region of the mass spectrometer 20 cm apart. A 100,000 Da particle in such a hypothetical pulse will arrive at the ionization region approximately 85 μs after the carrier gas. But the actual pulse is 500 μs wide. Therefore, a 100 μs temporal delay will not cause mass discrimination in the ionization protocol, provided that the laser is fired at the proper time to intercept the central portion of the aerosol pulse. Under these conditions, the ionizing 20 ns long laser pulse virtually probes a semi continuous aerosol pulse. Our experience indicates that the relative mass distribution is insensitive to the delay time between the laser and the aerosol pulse within a few hundred microseconds range.

The effect of the initial velocity distribution on mass calibration is negligible compared to the uncertainty due to the limited resolution. Typical neutral velocities correspond to energies on the order of a few thousand volts for a MDa particle, which amounts only to 1% of the energy added by applying the electric field. It is estimated that such an effect will introduce a mass calibration error if resolution is ~ 600 , a value much higher than the instrumental resolution of 40.

A promising approach to increase the high-mass detection limit while improving the instrumental resolution is to use an alternative method for particle fragmentation. In principle, it should be possible to evaporate single atoms from large particles using a continuous high-intensity electron gun. The approach of detecting lighter fragments originating from massive particles could lead to the efficient mass-unlimited detection using lower operating voltages. Such approach will result in a higher mass resolution. In fact, the method has been successfully used to measure the mass content of large particles once the particles are sized with alternative techniques (Sinha and Friedlander, 1985). Alternatively, similar to the laser ablation schemes employed for detecting micron-size particles, it should be possible to use a second laser synchronized with the ionization laser to ablate ion packets of a given mass. By doing so, the elemental and molecular composition of particles may be obtained together with improved resolution in detecting massive particles.

APPLICATIONS

Characterizing a nanocrystal flow processor

Characterizing the performance of an aerosol source has been a challenging enterprise. It involved the production of particles in the desired size range, subsequent collection in

a suitable solvent or substrate, careful deposition onto electron microscope grids, and imaging with an electron microscope (Granqvist and Burhman, 1976). Since each step is repeated every time a parameter in the aerosol source is changed, the process is quite tedious and time consuming, usually involving analysis time scale of weeks. Furthermore, great care has to be exercised not to expose the particles to detrimental atmospheres such as air, light, or solvents, since small particles are often highly reactive. The device described here greatly simplifies the characterization task by allowing the continuous monitoring of particle size, as important operating parameters are systematically changed.

Residence time

One of the most important and easily controlled parameters governing particle growth in aerosol processors is the time during which a particle condensates before its growth is arrested. To determine its effect on Na particle size in the NXFP described in Fig. 2, the residence time was systematically changed by adjusting the carrier gas flow rate while maintaining the Na furnace temperature constant. An excess dilution flow rate of 10 slpm was maintained throughout the experiment to prevent aerosol coagulation during its expansion from the aggregation cell exit nozzle to the sampling location, distance of 12 cm. The results are shown in Fig. 4. Clearly, the particle size varies linearly with residence time. This behaviour is consistent with what is observed in other lower pressure gas aggregation sources (Mann and Broida, 1971; Zimmermann *et al.*, 1994). This is not a surprising result since these sources operate on principle of particle aggregation by collisions with monomer units. Therefore, it is reasonable to expect that the faster a growing particle moves through aggregation region the fewer collisions it is experiencing. A simplified quantitative model explaining these observations has been proposed by Alvarez (Alvarez, 1995). Examination of the mass spectra (not shown) reveals that the size distribution is fairly wide, amounting on average to 50% mass dispersion below the mean mass, and 60% above the mean mass, as determined by inspecting FWHM of the mass spectra peaks.

Effect of dilution

Once an aerosol of a given size distribution has been prepared, it is important to prevent particle coagulation. Typically this is accomplished by diluting the aerosol with excess He.

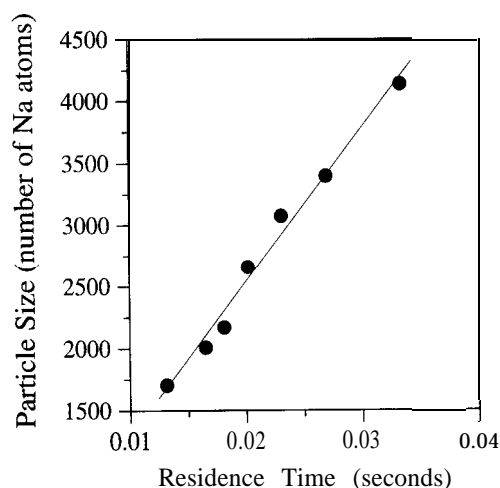


Fig. 4. Average particle size increases linearly with increasing carrier gas residence time in the aggregation cell. These measurements were performed by fixing the Na oven temperature constant at 340°C (0.02 mbar vapor pressure) and the dilution flow rate at 16 slpm, while adjusting the source flow rate between 2.7 and 6.9 slpm. The solid line is a linear fit though the data points ($N = 35 + 1.2 \times 10^5$ atoms/s). The aggregation cell volume is 1.5 ml. Geometric diameter changes from 5-7 nm.

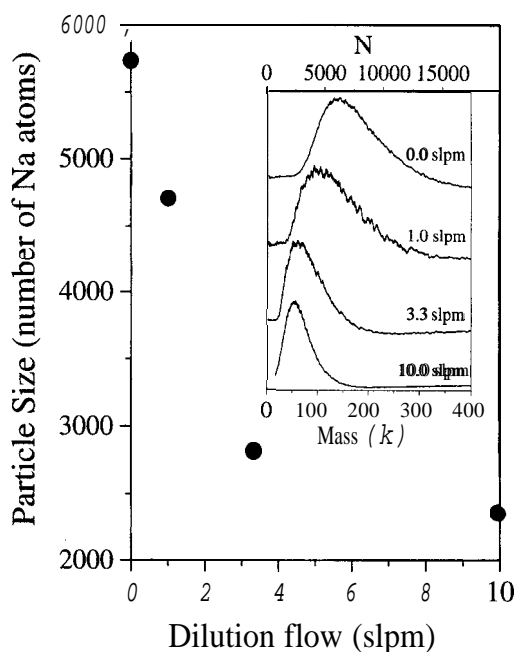


Fig. 5. Role of a dilution by secondary He flow in preventing particle coagulation. Inset shows corresponding mass spectra at various dilutions. Source flow and temperature were fixed at 1 slpm and 234°C, respectively. Sizes extracted from mass spectra correspond to a diameter range of 5-8 nm.

Figure 5 depicts a series of size distributions for Na nanocrystals at various dilution flows, as obtained by sampling the aerosol to a mass spectrometer. If undiluted, a 2400-atom Na aerosol (6 nm mean particle diameter) flowing at 1 slpm can grow in excess of twice its size. However, if at least threefold diluted, particle growth is arrested as seen by the insensitivity of particle size to further dilution increase. This result is important because it enables the subsequent processing of the aerosol, namely annealing, etching, and passivation, while preserving its original size distribution. The mass spectrum (Fig. 5 inset) shows that the long mass tail of undiluted case increases dramatically in contrast to the low mass region, which remains fairly constant for all but the extreme case of no dilution. These results indicate that the main growth mechanism of pre-formed particles is through particle-particle collisions rather than by monomer addition.

A reacting sodium aerosol

To demonstrate real-time aerosol dynamics, the gas-phase reaction



where $\text{R} \equiv \text{C}_{12}\text{H}_{25}$ is performed. This reaction illustrates the use of surfactants or passivating agents to quench particle growth. The experimental setup discussed allows the reaction to be monitored in real-time. Nanocrystals are produced in the source section (Fig. 2) of the aerosol processing device (A). The aerosol source conditions, furnace temperature, pressure, flow rate are controlled so that a mean particle size of 7900 Na atoms (8 nm diameter) is maintained throughout the experiment. The particle size is verified by sampling a dilute neat (no thiol) stream into the mass spectrometer. A He stream saturated with thiol at a preset vapor pressure was generated by flowing He through a passivation cell (B). The thiol is heated in an annular container around the He flow channel and is evaporated into the flowing He stream. The carrier gas is preheated to the thiol evaporation temperature to ensure thermal equilibrium within the stream, and to keep the vaporization temperature

constant. The stream meets the nanocrystal aerosol coaxially to enhance immediate mixing. The mixing happens in the dilution piece (C), where reaction starts. The product is sampled into the mass spectrometer vacuum system via a molecular beam valve (D) 10 cm from the point of mixing. Under described conditions, total flow of aerosol is 13 slpm, so the reaction lasts for approximately 0.02 s. The sampled aliquot is not reacting since it is rarefied upon expansion into vacuum.

The experiment consists of systematically increasing the temperature of the thiol source from 40°C to 160°C. A thiol vapor pressure change from 0.02 to 28 mbar (Reid, 1958), corresponding to increase in thiol mole fraction in the carrier gas from 2.6×10^{-5} to 0.02 before mixing with the Na aerosol. In the nanocrystal source 1 mbar of atomic Na is evaporated into the atmospheric He stream. Since the mean nanocrystal size is 7900 atoms, the partial pressure is approximately 1.3×10^{-6} mbar or mole fraction of 1.7×10^{-7} . Between temperature increments, the system is allowed to reach steady state conditions, as judged by monitoring the mass spectra of the reacting mixture.

The results of the Na-thiol experiment are summarized in Fig. 6 which depicts how the thiol/Na mole ratio in the particle changes with thiol vapor pressure. The corresponding evolution of the mass spectrum is shown as well. The first striking feature is that particles grow monotonically with increasing thiol mole fraction in the reacting stream. The crystal is not etched as might be expected from the stability of a Na mercaptide monomer. Energetically, it may be more favorable to have N mercaptide molecules than an N-atom Na particle bound to N-m thiol molecules and m extra free thiols in the aerosol. However, before the system can reach this preferred state, it must break many bonds posed by the reduction in the particle's surface implied by the removal of Na surface atoms. On the contrary, thiols effectively act as surfactants by stabilizing the exposed Na atoms at the surface, which are generally the most energetically unfavored due to unsatisfied coordination and dangling bonds. This result is significant because it shows that a pre-formed particle can indeed be passivated with ligands which may otherwise destroy it. In

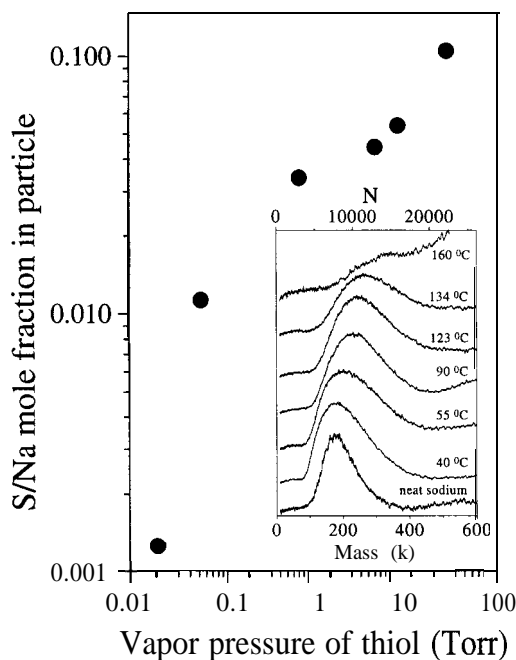


Fig. 6. An atmospheric Na nanocrystal ca. 8000 atoms or 8 nm in diameter flowing at 2.7 slpm reacts with a lauryl mercaptan stream at 10 slpm. Mass spectra are labeled by the temperature of the thiol crucible corresponding to thiol vapor pressures of 0, 0.02, 0.06, 0.71, 4.7, 8.3, and 28 mbar from bottom to top. The Na temperature was constant at 400°C (0.4 mbar vapor pressure).

addition, the results in Fig. 6 show that particles grow in a manner consistent with a complete coverage of their surfaces with thiols. A spherical 7900-atom particle (diameter of 8 nm), has roughly 18% (1400) of its atoms on the surface. If the same type of bonding observed between thiols and bulk noble metals surfaces is assumed, 1 thiol per 2–3 host atoms (Camillone *et al.*, 1993), then a 7900-atom particle will be fully enclosed with a thiol monolayer of 500–700 thiol molecules (669% of thiols per total Na atoms). Significantly, the observed S to Na mole fraction reaches a plateau between 5–6%, implying that the particle is indeed passivated by the condensation of a closely packed surfactant layer on its surface. The subsequent mass increase beyond monolayer coverage is presumably due to the condensation of less strongly bound additional thiol layers onto the passivated particles. It is indeed possible that those particles survive the mass analysis protocol as long as the laser ionization is soft. However, the lack of data at higher masses does not allow a final conclusion in this respect. Nevertheless, the fact that it is possible to follow changes in particle mass in real-time, and that the results agree with expectations on how a particle should react with thiols, demonstrates that the technique described here has a great potential as an in situ monitoring technique of aerosol processes in general.

CONCLUSIONS

The on-line aerosol sampling and mass analysis protocol described herein enable the sampling and mass characterization of submicron, namely 1–10 nm in diameter aerosols flowing at atmospheric pressures at 10^{10} cm^{-3} concentrations. The setup allows the detection of aerosol processes in the millisecond time range. The sensitivity of the instrument is limited by the necessity of diluting the aerosol to prevent particle aggregation, by the photoionization efficiency, and by the mass spectrometer detector. In its present stage, the instrument applicability is limited to those materials with work functions less than 6.4 eV. The capability of the instrument to follow real-time aerosol changes was demonstrated by studying the effect of residence time and dilution flow on particle size in an aerosol processor, and the reaction between Na nanocrystals and dodecyl mercaptan in the gas phase.

In reference to differential mobility sizing methods, the technique described in this work suffers from poor absolute sensitivity, strong sensitivity to particle composition in the photoionization process, and its limited capability to provide particle composition information since, in general, particles are detected intact (total mass determination). Particle fragmentation may be induced by increasing the fluence of ionization laser, thus yielding information on its elemental and molecular constituents. In addition, the information on geometrical size is limited since a particle density and shape must be assumed in order to extract sizes from weights. Nevertheless, as demonstrated above, these deficiencies are compensated by the ability of the method to follow instantaneous changes in aerosol processes, and to detect particles from 10 nm diameter to the atomic dimensions, a range inaccessible to conventional sizing techniques. The low pumping requirements are beneficial as well.

Finally, the following modifications are conceivable to improve the instrument's sensitivity and extend its capabilities: (i) the replacement of the valve's divergent conical expansion nozzle with a straight channel expansion piece in order to define the sampled aerosol into a narrow, more dense beam; (ii) the use of a non-selective method of ionization such as a vacuum ultraviolet light source or an electron impact ionization source; (iii) the use of alternate particle fragmentation schemes as opposed to particle/dynode collisions, such as a continuous electron or laser beam; (iv) the use of conversion dynode materials with higher photoelectron yields (alkali halide surfaces, alkali metals, alkaline earth metals); (v) in analogy to the schemes for micron-sized particles, the use of a second ablation laser synchronized with the ionization event to ablate particles of a given size, thus providing a simultaneous complete mass spectrum in addition to its total mass content.

REFERENCES

- Alvarez, M. M. (1995) Ph.D. Thesis. University of California, Los Angeles.
- Arpino, P. J. (1995) Mass spectrometry combined with other methods. In *Advances In Muss Spectrometry*, Vol. 13 (Edited by Eötvös, I. C. and Horvath, G.), p. 151. Wiley, Budapest.
- Bahat, K., Cheshnovsky, O., Even, U., Lavie, N. and Magen, Y. (1987) Generation and detection of intense cluster beams. *J. Phys. Chem.* 91, 2460–2462.
- Burtscher, H. and Siegmann, H. C. (1994) Aerosols, large clusters in gas suspensions. In *Clusters of Atoms und Molecules II* (Edited by Haberland, H.), p. 272. Springer, New York.
- Camillone III, N., Chidsey, C. E. D., Liu, G. and Scoles, G. (1993) Substrate dependence of the surface structure and chain packing of dicosyl mercaptan self-assembled on the (111), (110), and (100) faces of single crystal gold. *J. Chem. Phys.* 98, 4234.
- Carson, P. G., Neubauer, K. R., Johnston, M. V. and Wexler, A. S. (1995) On-line chemical analysis of aerosols by rapid single-particle mass spectrometry. *J. Aerosol Sci.* 26, 535–545.
- Cotter, R. J. (1992) *Time-of-Flight Muss Spectrometry*. American Chemical Society, Washington, DC.
- Daley, N. R. (1960) *Rev. Sci. Instrum.* 31, 264.
- de Heer, W. A. (1993) The physics of simple metal clusters: experimental aspects and simple models. *Rev. Mod. Phys.* 65, 611–676.
- Granqvist, C. G. and Burhman, R. A. (1976) Ultrafine metal particles. *J. Appl. Phys.* 47, 2200.
- Guilhaus, M. (1995) The return of time-of-flight to analytical mass spectrometry. In *Advances in Mass Spectrometry*, Vol. 13 (Edited by Eötvös, I. C. and Horvath, Gy.), p. 213. Wiley, Budapest.
- Haberland, H. (1994) Experimental methods. In *Clusters of Atoms and Molecules I*. (Edited by Haberland, H.), p. 207, Springer, New York.
- Hinz, K. P., Spengler, B. and Kaufmann, R. (1995) On-line size and composition analysis of particles from ambient aerosols by laser mass spectrometry. *J. Aerosol Sci.* 26, S65–S66.
- Kaye, B. H. and Trotter, R. (1995) The many measures of fine particles. *Chem. Engr.* 102, 78–86.
- Kroto, H. W., Heath, J. R., O'Brien, S. C., Curl, R. F. and Smalley, R. E. (1985) C₆₀ Buckminsterfullerene. *Nature* 318, 162–165.
- Makela, J. M. and Jokinen, V. (1994) Ion mobility measurements by a Vienna type DMA and Faraday cup electrometer. *J. Aerosol Sci.* 25, S541–S542.
- Mann, D. M. and Broida, H. P. (1971) *Phys. Rev. Lett.* 26, 1236.
- Marijnissen, J., Scarlett, B., Verheijen, P. (1988) Proposed on-line aerosol analysis combining size determination, laser-induced fragmentation and time-of-flight mass spectroscopy. *J. Aerosol Sci.* 19, 1307.
- Mark, T. D. and Echt, O. (1994) Internal reactions and metastable dissociations after ionization of van der Waals clusters. In *Clusters of Atoms and Molecules II*. (Edited by Haberland, H.), p. 154. Springer, New York.
- McKeown, P. J., Johnston, M. V. and Murphy, D. M. (1991) On-line single-particle analysis by laser desorption mass spectrometry. *Anal. Chem.* 63, 2069.
- Murray, K. K., Lewis, T. M., Beeson, M. D. and Russell, D. (1994) Aerosol matrix-assisted laser desorption ionization for liquid chromatography/time-of-flight mass spectrometry. *Anal. Chem.* 66, 1601–1609.
- Nordmeyer, T. and Prather, K. A. (1994) Real-time measurement capabilities using aerosol time-of-flight mass spectrometry. *Anal. Chem.* 66, 3540–3542.
- Reents, W. D., Downey, S. W., Emerson, A. B., Muijsce, A. M., Muller, A. J., Siconolfi, D. J., Sinclair, J. D. and Swanson, A. G. (1995) Single-particle characterization by time-of-flight mass spectrometry. *Aerosol Sci. Technol.* 23, 263.
- Reid, E. E. (1958) *The Organic Chemistry of Bivalent Sulfur*. Chemical Publishing Co., New York.
- Reilly, P. T. A., Gieray, R. A., Yang, M., Whitten, W. B., Ramsey, J. M. (1997) Tandem mass spectrometry of individual airborne microparticles. *Anal. Chem.* 69, 36–39.
- Sattler, K. and Muhlbach, J. (1980) Electronic time of flight mass spectrometer and separator for metal clusters. *J. Phys. E: Sci. Instrum.* 13, 6733661.
- Schmidt-Ott, A. (1994) Characterizing and classifying ultrafine aerosol particles. *J. Aerosol Sci.* 25, S559–S560.
- Siegmund, O. H. W. and Malina, R. (1983) Detection of extreme uv and soft X-rays with microchannel plates: a review. In *Multichannel Image Detectors 2* (Edited by Talmi, Y.), pp. 2533275. American Chemical Society, Washington, D. C.
- Sinha, M. P. and Friedlander, S. K. (1985) Real-time measurement of sodium chloride in individual aerosol particles by mass spectrometry. *Anal. Chem.* 57, 1880–1883.
- Thomson, D. S. (1994) Analyzing single aerosol particles in real-time. *Chem. Tech.* 24, 30–35.
- Ulman, A. (1991) *An Introduction to Ultrathin Organic Films. From Langmuir Blodgett Films to Self Assembly*. Academic Press, Boston.
- Vezmar, I., Alvarez, M. M., Khoury, J. T., Salisbury, B. E. and Whetten, R. L. (1997) Cluster beams from passivated nanocrystals. *Z. Phys. D.* (accepted for publication).
- Wang, S. C. and Flagan, R. C. (1990) Scanning electrical mobility spectrometer. *Aerosol Sci. Technol.* 13, 230–240.
- Weber, R. J., McMurry, P. H., Eisele, F. L. and Tanner, D. J. (1995) Measurement of expected nucleation precursor species and 3-500 nm diameter particles at Mauna Loa observatory, Hawaii. *J. Atmos. Sci.* 52, 2242–2257.
- Weiss, M., Verheijen, P. J. T., Marijnissen, J. C. M. and Scarlett, B. (1995) On-line tof-mass spectrometry of aerosols: system characterization. *J. Aerosol Sci.* 26, s101–s102.
- Whetten, R. L. (1993) Processing of single nanocrystals. *Mater. Sci. Eng.* B19, 8813.
- Wiedensohler, A., Aalto, P., Covert, D., Heintzenber, J. and McMurry, P. H. (1994) Intercomparison of four methods to determine size distributions of low-concentration ($\sim 100 \text{ cm}^{-3}$), ultrafine aerosols ($3 < D_p < 10 \text{ nm}$) with illustrative data from the Arctic. *Aerosol Sci. Technol.* 21, 95–109.
- Winklmayr, W., Reischl, G. P., Lindner, A. O. and Berner, A. (1991) A new electromobility spectrometer for the measurement of aerosol size distributions in the size range from 1 to 1000 nm. *J. Aerosol Sci.* 22, 289–296.
- Ziemann, P. J., Liu, P., Rao, P., Kittelson, D. B. and McMurry, P. H. (1995) Particle beam mass spectrometry of submicron particles charged to saturation in an electron beam. *J. Aerosol Sci.* 26, 7455756.
- Zimmermann, U., Malinowski, N., Näher, U., Frank, S. and Martin, T. P. (1994) Producing and detecting large clusters. *Z. Phys. D.* 31, 85593.